J. Chem. Sci. Vol. 128, No. 1, January 2016, pp. 133–139. © Indian Academy of Sciences.
DOI 10.1007/s12039-015-1011-y

Highly selective detection of Zn^{2+} and Cd^{2+} with a simple amino-terpyridine compound in solution and solid state

DUOBIN CHAO
School of Petroleum and Chemical Engineering, Dalian University of Technology, Panjin, Liaoning 124221, P. R. China
e-mail: chaoduobin@dlut.edu.cn

MS received 22 July 2015; accepted 17 November 2015

Abstract. A simple amino-terpyridine sensor exhibits highly selective detection of Zn^{2+} and Cd^{2+} in solution and solid state based on the intramolecular charge transfer (ICT) effect. The detection limits were determined to be 0.184 μM for Zn^{2+} and 0.176 μM for Cd^{2+}. Job's plot experiments suggest a 1:1 binding mode between the sensor and metal ions like Zn^{2+} and Cd^{2+}. The resulting complexes were found to be emissive in solution and solid state.

Keywords. Terpyridine; sensor; Zn^{2+}; Cd^{2+}; ICT.

1. Introduction

Detection of metal ions has attracted much attention due to their significant impact on the environment and human body.[1–3] Some metal ions play an important role in the human body and are involved in various biological processes. For example, Zn^{2+} is the second most abundant transition metal ion in the human body and is important for immune function, brain function and pathology, gene transcription and mammalian reproduction.[4–6] However, some metal ions may be highly toxic in nature and for human body. For example, Cd^{2+} has been widely used in industry and agriculture, and may be taken in by human body through food or water.[7] Then it may cause some diseases such as prostate cancer and renal dysfunction.[8] Therefore, it is meaningful to develop efficient methods for the detection of Zn^{2+} and Cd^{2+}.

Fluorescent sensors for the detection of Zn^{2+} and Cd^{2+} have been studied in many reports because of simplicity, sensitivity and inexpensiveness, and several sensing mechanisms such as photo-induced electron transfer (PET) and intramolecular charge transfer (ICT) are well–established.[9–12] However, fluorescent sensors with different fluorescence response to Zn^{2+} and Cd^{2+} are rare.[13] This is probably because they have similar electron configuration. It is still challenging and urgently needed to develop efficient fluorescent sensors for the detection of Zn^{2+} and Cd^{2+} with high selectivity and sensitivity.

2,2′:6′,2″–terpyridine and their derivatives are well–known for their excellent coordination ability with various metal ions, and these compounds have attracted a lot of attention in the fields of coordination and supramolecular chemistry as well as in materials science.[14–17] However, terpyridines also exhibit excellent photophysical properties with tunable emission color and quantum yields by introducing different group on terpyridine structure, especially in the 4′ position.[18] 4′–substituted terpyridines usually exhibit ICT effect, and the efficiency of ICT may be tuned by the substituted group or coordination with metal ions. Thus, emission color and quantum yields of 4′–substituted terpyridines may be varied in the presence of different metal ions and be used as fluorescent sensors for the detection of metal ions based on the ICT mechanism. Although there have been several terpyridines reported for the detection of metal ions, their synthesis was complicated with several steps.[19,20]

The interaction between metal ions and **1** (scheme 1) was studied before,[21–23] but its application in the detection of Zn^{2+} and Cd^{2+} in solution and solid state is studied here in detail for the first time. Their complexes were characterized and found to be emissive in solution and solid state. Complexes **2** and **3** exhibit yellow emission in solid, while **4** and **5** exhibit green emission in solid (structures in scheme 1).

2. Experimental

2.1 *Materials and Methods*

All the solvents and reagents for synthesis were purchased from commercial suppliers and used

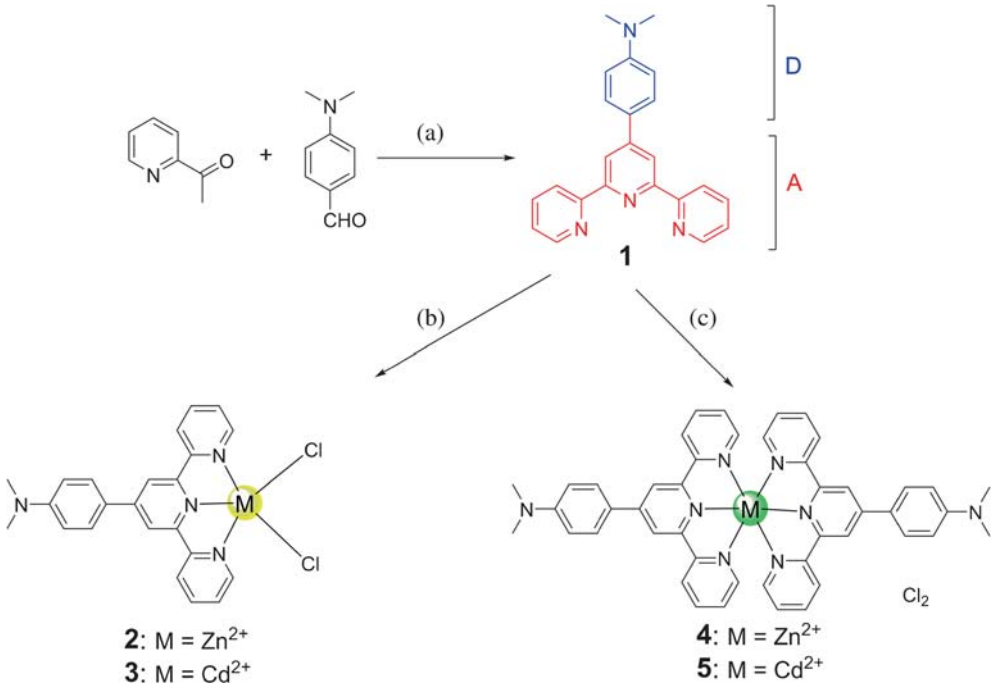

Scheme 1. Reaction conditions: (a) [24]KOH, C_2H_5 OH, aq. NH_3, rt; (b) 1 equv. $ZnCl_2$ or $CdCl_2$, DMF, 40°C; (c) 0.5 equv. $ZnCl_2$ or $CdCl_2$, DMF, 90°C.

without further purification. Sensor **1**[24] was synthesized and characterized as reported. ^{1}H NMR spectra were recorded using a Bruker Avance DPX 300 MHz instrument with tetramethylsilane (TMS) as an internal standard. ESI–MS spectra were recorded using a Thermofisher Q–Exactive instrument. UV–Vis absorption spectra were recorded with Perkin Elmer Lambda 950 spectrometer. Steady emission spectroscopy was measured by Lengguang Tech. Instruments (F97PRO) with Xe lamp as the light source. All calculations were performed with the Gaussian 09 program package employing the density functional theory (DFT) method with B3LYP/6-31G(d) level for C, H, N, O, Cd atom and B3LYP/LANL2DZ for Zn atom.[25] The compound **1** stock solution (10^{-3}M) was prepared by dissolution in DMSO. Stock solutions of Na^+, Fe^{2+}, Co^{2+}, Ni^{2+}, Zn^{2+}, Cd^{2+}, Cu^{2+}, Mn^{2+}, and Pb^{3+} in THF were also prepared. For the UV-Vis and fluorescence analysis, the stock solution of **1** in DMSO was diluted to 10^{-5} M in THF. All the measurements were carried out at 298 K.

2.2 *Synthesis of compounds*

Complexes **2, 3, 4** and **5** were prepared in a general way (Scheme 1): $ZnCl_2$ or $CdCl_2$ (0.14 mmol for **2** and **3**, 0.07 mmol for **4** and **5**) was added into **1** (0.14 mmol) in DMF (10 mL) and the resulting suspension solution stirred (40°C for **2** and **3**, 90°C for **4** and **5**) for 3 h. The precipitate was filtered, washed with water, methanol, and diethyl ether. Then the pure product was obtained after dried under vacuum.

2.2a *Complex **2***: Yield: 60%. ^{1}H NMR (500 MHz, DMSO-d_6), δ (ppm): 8.90 (m, 4H), 8.81 (d, 2H, J = 4.0 Hz), 8.30 (td, 2H, J = 7.5 Hz), 8.20 (d, 2H, J = 5.0 Hz), 7.85 (m, 2H), 6.86 (d, 2H, J = 5.0 Hz), 3.07 (s, 6H). ESI-MS: m/z 451.06 for $[M\text{-}Cl]^+$ (calcd for $C_{23}H_{20}ClN_4Zn$ m/z 451.06)

2.2b *Complex **3***: Yield: 55%. ^{1}H NMR (500 MHz, DMSO-d_6), δ (ppm): 8.89 (m, 4H), 8.74 (m, 2H), 8.30 (s, 2H), 8.17 (s, 2H), 7.86 (s, 2H), 6.86 (d, 2H, J = 10.0 Hz), 3.05 (s, 6H). ESI-MS: m/z 501.04 for $[M\text{-}Cl]^+$ (calcd for $C_{23}H_{20}ClN_4Cd$ m/z 501.04)

2.2c *Complex **4***: Yield: 40%. ^{1}H NMR (500 MHz, DMSO-d_6), δ (ppm): 8.96 (m, 8H), 8.82 (d, 4H, J = 5.0 Hz), 8.32 (td, 4H, 7.0 Hz), 8.23 (d, 4H, J = 9.0 Hz), 7.81 (m, 4H), 6.90 (d, 4H, J = 10.0 Hz), 3.08 (s, 12H). ESI-MS: m/z 384.13 for $[M\text{-}2Cl]^{2+}$ (calcd for $C_{40}H_{40}N_8Zn$ m/z 384.13)

2.2d *Complex **5***: Yield: 43%. ^{1}H NMR (500 MHz, DMSO-d_6), δ (ppm): 8.94 (m, 8H), 8.76 (d, 4H, J = 4.5 Hz), 8.20 (m, 8H), 7.86 (s, 4H), 6.89 (d, 4H, J = 10.0 Hz), 3.06 (s, 12H). ESI-MS: m/z 409.12 for $[M\text{-}2Cl]^{2+}$ (calcd for $C_{40}H_{40}N_8Zn$ m/z 409.12).

2.3 *Calculation of relative quantum yields*

The relative fluorescence quantum yields were measured using quinine sulfate solution ($\Phi = 0.54$, 0.1 M H_2SO_4) as the standard at room temperature. Samples and the standard were excited at the wavelength of 380 nm, and the absorbance was kept below 0.05. The quantum yields were calculated using eq. (1).

$$\Phi_s/\Phi_f = (A_s/A_f) \times (Abs_f/Abs_s) \times \left(\eta_s^2\right) / \left(\eta_f^2\right) \quad (1)$$

In eq. (1), Φ_s and Φ_f are the quantum yields of the standard (quinine sulfate in 0.1 M H_2SO_4) and samples (**1**, **1** + Cd^{2+} and **1** + Zn^{2+}) respectively; η_s and η_f are the solution refractive indices of the standard and reference, respectively; Abs_s and Abs_f are the absorbance of the standard and samples at the wavelength of excitation (380 nm)respectively; A_s and A_f are the emission areas of sample and the standard, respectively.

2.4 *Detection limit*

The detection limit was calculated using the following equation.

$$\text{Detection limit} = 3\sigma/k \quad (2)$$

where σ is the standard deviation of blank measurement,[26] and k is the slope between the ratio of fluorescence emission versus respective analyte concentration.

2.5 *Binding constant*

The binding constant (K_s) was determined using the Benesi-Hildebrand (B-H) plot (eq. 3) by plotting the fluorescence intensity versus the free Zn^{2+}or Cd^{2+}concentration.

$$\log\{(F - F_{min}) / (F_{max} - F)\} = \log K_s + \log C \quad (3)$$

In eq. (3), F_{min} is the fluorescence intensity of **1** (λ_{exc} = 380 nm, λ_{emi} = 470 nm) without the addition of analyte (Cd^{2+} or Zn^{2+}), F is the observed fluorescence intensity of **1** with the addition of a certain concentration of the analyte (C), F_{max} is the obtained fluorescence intensity of **1** after the addition of excess analyte, K_s is the binding constant.

2.6 *Job's plot*

The binding stoichiometry of compound **1** with Cd^{2+} or Zn^{2+} was investigated via a Job's plot according to the titration experiment of Cd^{2+} or Zn^{2+}, and the total concentration of the metal ion and **1** was kept as 42.6 μM.

2.7 *Fabrication of PMMA films*

5.0 mg of compound **1** was dissolved in 4.0 mL of CH_2Cl_2 containing 100.0 mg of PMMA. Then 0.3 mL of the resulting solution was coated onto the surface of thin quartz plate (0.8 × 10 cm^2). The solvent was then allowed to evaporate.

3. Results and Discussion

3.1 *Synthesis and characterization*

Sensor **1** and its complexes were synthesized as shown in scheme 1. The total synthesis process was facile and effective. Sensor **1** was obtained facilely with the –NMe_2 group as the electron donor (D) and terpyridyl moiety as the electron acceptor (A) (scheme 1). Thus, electrons probably mainly localize on the –NMe_2 group in the ground state and transfer to terpyridyl moiety in the excited state for sensor **1**. As shown in figure 1, both absorbance and fluorescence spectra of **1** exhibited significant bathochromic shifts with the increase of solvent polarity, which suggested photophysical properties of **1** were strongly influenced by solvent polarity. It is reasonable because the more polar solvent like CH_3CN

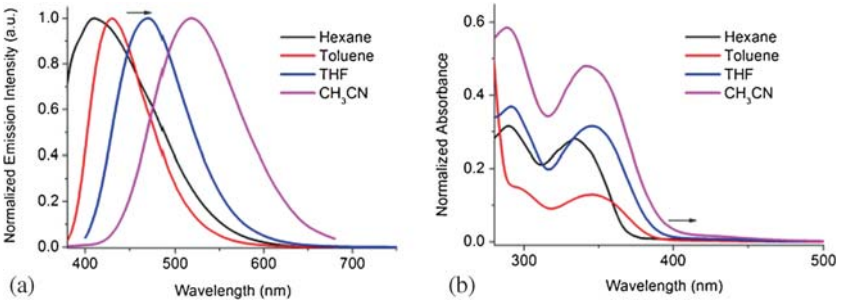

Figure 1. Normalized emission spectra (a) and absorption spectra (b) of sensor 1 in various solvents. The emission spectra were recorded at room temperature when excited at 380 nm.

can stabilize the charge transfer (CT) excited state of **1** more efficiently than the less polar solvent like THF.[9] Although the emission wavelength was red shifted by 49 nm in CH_3CN compared with that in THF, the quantum yield decreased to 0.227 (0.429 in THF). Considering all the above issues, the absorbance and fluorescence spectra of **1** in presence of metal ions were studied to examine the detection of Zn^{2+} and Cd^{2+} in THF and in solid.

3.2 *Fluorescence spectroscopic studies of **1** in the presence of Zn^{2+} and Cd^{2+}*

To study the detection of Zn^{2+} and Cd^{2+} with sensor **1**, the fluorescence emission spectra of sensor **1** upon addition of Zn^{2+} and Cd^{2+} were first recorded in THF at room temperature. As shown in figure 2, the sensor **1** exhibited structureless and strong emission at 470 nm before the addition of Zn^{2+} and Cd^{2+}. However, the emission at 470 nm gradually decreased and the new emission peak at 535 nm appeared with the titration of Zn^{2+}, and the fluorescence quantum yield was reduced to 0.272. As a result, the strong blue emission of sensor **1** turned to the weaker yellowish–green emission in presence of Zn^{2+}. With the titration of Cd^{2+}, the emission at 470 nm also decreased and a new emission peak at 551 nm appeared. The quantum yield was reduced to 0.134 and the blue emission turned to yellow emission after the addition of Cd^{2+}. These results revealed that sensor **1** may distinguish Zn^{2+} and Cd^{2+}

In order to know more about the detection of Zn^{2+} and Cd^{2+} with sensor **1**, more titration experiments were performed. The emission intensity at 470 nm was found to be decreased almost linearly with the increase of Zn^{2+} and Cd^{2+} (figures S1 and S2 in Supplementary Information). The detection limits were determined to be 1.84×10^{-7} M and 1.76×10^{-7} M for Zn^{2+} and Cd^{2+}, respectively. Job's plot experiments were also performed to reveal the possible binding ratio between sensor **1** and metal ions which was found to be 1:1 for Zn^{2+} and Cd^{2+} (figures S5 and S6 in SI). In addition, the binding constants were determined to be 3.29×10^6 M^{-1} and 5.37×10^6 M^{-1} for Zn^{2+} and Cd^{2+} respectively (figures S3 and S4 in SI).

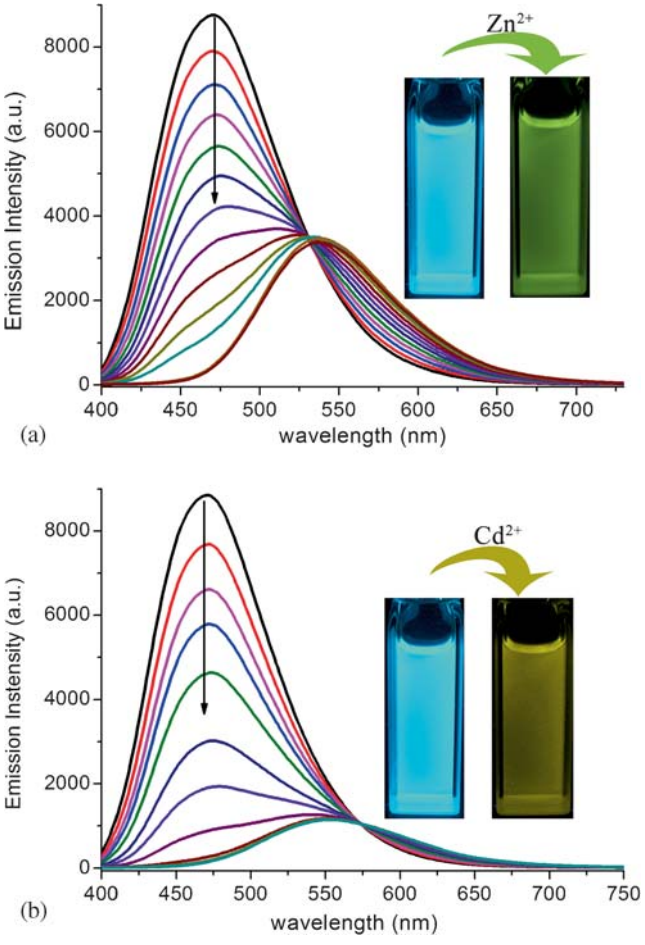

Figure 2. Fluorescence emission titration of sensor 1 (42.6 μM) upon addition of Zn_{2+} (0–50 μM) (a) and Cd_{2+} (0–50 μM) and (b) in THF at room temperature when excited at 380 nm. Insets: the photographs of 1 after addition of Zn_{2+} (a) and Cd_{2+} (b) under a 365 nm UV lamp.

3.3 *UV-Vis spectroscopic studies of **1** in the presence of Zn^{2+} and Cd^{2+}*

Uv–Vis titration experiments were conducted for Zn^{2+} and Cd^{2+} as shown in figure 3 and figure S7 (in SI). It is worth noting that there are several isobestic points upon titration of Zn^{2+} and Cd^{2+}. For the titration experiment

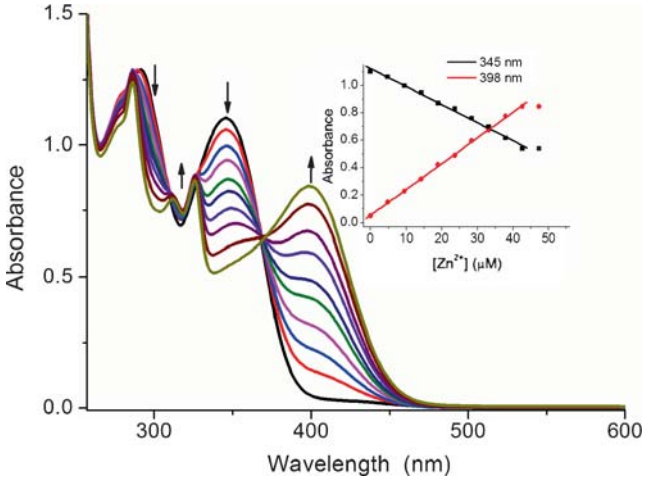

Figure 3. UV–Vis titration of sensor 1 (42.6 μM) upon addition of Zn_{2+} (0–50 μM) in THF at room temperature. Inset: absorbance observed at 345 nm and 398 nm as a function of the concentration of Zn_{2+}.

of Zn^{2+}, the absorption band at 345 nm decreased and the absorption band at 398 nm increased. This red shift may be attributed to coordination between sensor **1** and Zn^{2+}, because the Zn^{2+} coordinated to **1** enhances the electron–withdrawing ability of terpyridyl moiety in **1**. In addition, the absorption spectrum remained nearly constant after the ratio of amount of Zn^{2+}/**1** was over 1, indicating that the binding mode for **1** and Zn^{2+} is 1:1. Similar tendency was also observed for the addition of Cd^{2+} to **1**

3.4 *Detection of Zn^{2+} and Cd^{2+} in solid state*

To explore the practical application of senor **1** in the detection of Zn^{2+} and Cd^{2+}, sensor **1** was embedded with PMMA. As shown in figure 4(c), a drop of Zn^{2+} and Cd^{2+} solution changed fluorescence of PMMA film from blue to yellow. This indicates sensor **1** in solid state can be used to detect Zn^{2+} and Cd^{2+}. To know more about the process, reactions for sensor **1** with Zn^{2+} and Cd^{2+} were conducted in 1:1 and 2:1 ratio respectively. All four complexes exhibit fluorescence in solid in figure 4(b). Complexes **2** and **3** exhibit yellow emission, but complexes **4** and **5** exhibit green emission. This suggests sensor **1** binds with Zn^{2+} and Cd^{2+} in 1:1 ratio.

3.5 *Selectivity*

Fluorescence response to other metal ions such as Cr^{3+}, Pb^{2+}, Co^{2+}, Cu^{2+}, Fe^{2+}, Ni^{2+}, Na^{+}, Hg^{2+} and Mn^{2+} were also performed to investigate the selective detection of Zn^{2+} and Cd^{2+} using sensor **1**. As shown in figure 5, in the presence of Cr^{3+}, Pb^{2+} and Na^{+}, the fluorescence spectra exhibit no significant change in the emission intensity. However, metal ions such as Fe^{2+}, Mn^{2+} and Cu^{2+} quenched the fluorescence obviously. In addition, Co^{2+}, Hg^{2+} and Ni^{2+} also quenched the fluorescence a lot with slight red shift. Zn^{2+} and Cd^{2+} show similar yellow emission, whereas the emission is

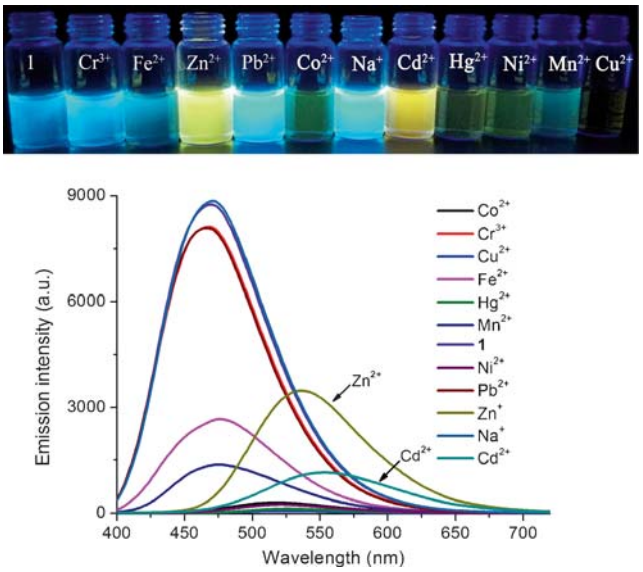

Figure 5. Fluorescence emission responses of sensor 1 (42.6 μM) towards various metal ions (60 μM) in THF at room temperature. Top: the photograph of 1 in the presence of various metal ions under a 365 nm UV lamp. Bottom: the emission spectra of 1 in the presence of various metal ions when excited at 380 nm.

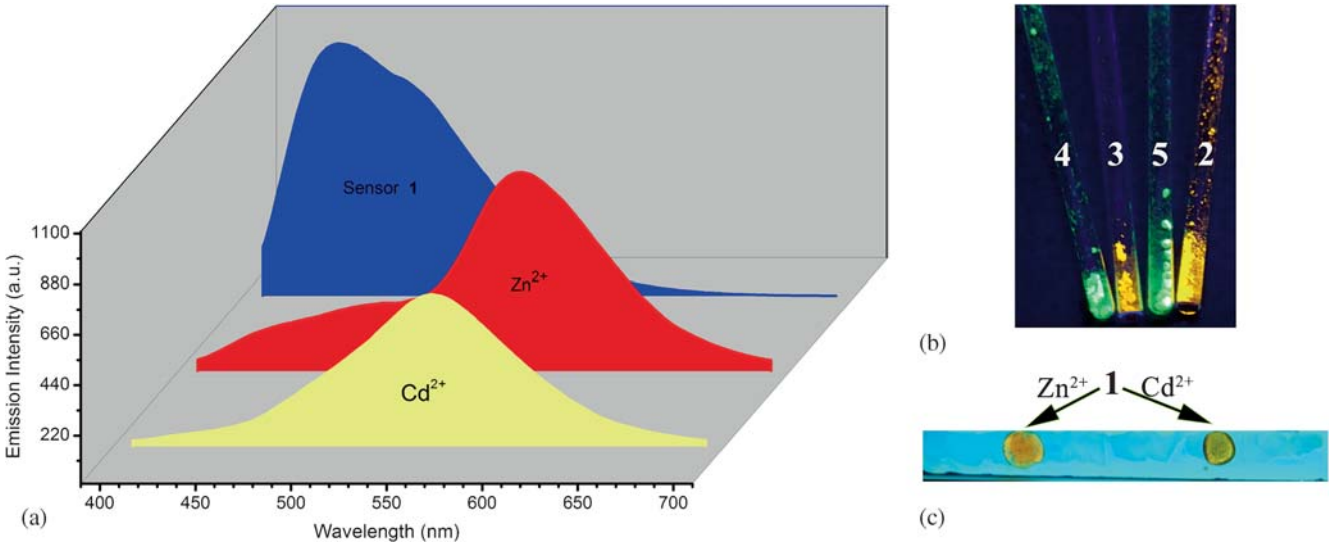

Figure 4. (a) Fluorescence emission spectra of sensor 1, after addition of Zn_{2+} and addition of Cd_{2+} in PMMA film, (b) the photograph of compounds 2, 3, 4, 5 in solid under a 365 nm UV lamp, (c) the photograph of sensor 1 in PMMA film after addition of Zn_{2+} and Cd_{2+} under a 365 nm UV lamp.

stronger in the presence of Zn^{2+}. It is worth noting that Cu^{2+} almost (∼100%) quenched fluorescence of sensor **1** probably due to the paramagnetic property of Cu^{2+} in d^9 configuration. These results indicate that **1** shows good selectivity for the detection of Zn^{2+} and Cd^{2+}.

3.6 *Theoretical studies*

To gain insight into the mechanism for the detection of Zn^{2+} and Cd^{2+} using sensor **1**, theoretical calculations for sensor **1** and its complex with Zn^{2+} (**1**–Zn) and Cd^{2+} (**1**–Cd) were performed in the framework of the DFT. As shown in figure 6, the HOMO of sensor **1** is mainly located on the $–NMe_2$ group and the LUMO is mainly located on the terpyridyl moiety, indicating intramolecular charge transfer from the $–NMe_2$ group to the terpyridyl moiety, and this is consistent with the above experimental results of the UV–Vis study of sensor **1**. Similarly, HOMOs of **1**–Zn and **1**–Cd are also located mainly on the $–NMe_2$ group, while LUMOs located partially on the Zn^{2+} for **1**–Zn and mainly on the Cd^{2+} for **1**–Cd. The calculated LUMOs of **1**–Zn and **1**–Cd are significantly lower than that of sensor **1**, which suggests

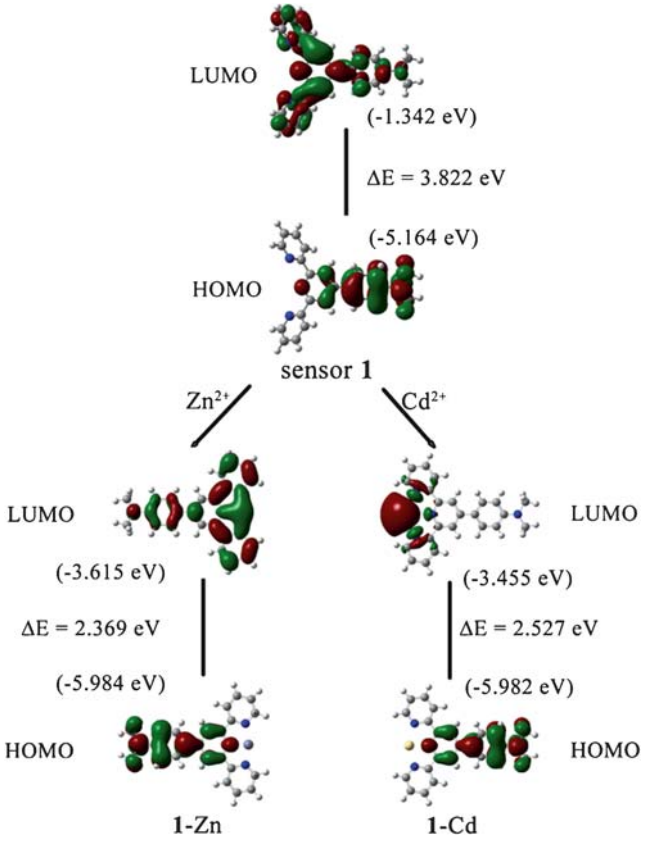

Figure 6. Energy diagrams of HOMO and LUMO of sensor 1 and complexes with Zn_{2+} (1–Zn) and Cd_{2+} (1–Cd).

that Zn^{2+} and Cd^{2+} coordinated with the terpyridyl moiety and stabilized the excited states of the complexes. Meanwhile, the calculated energy gaps of **1**–Zn and **1**–Cd are similar and smaller than that of sensor **1**, indicating the red shift of the emission wavelength of sensor **1** after coordination with Zn^{2+} and Cd^{2+}. It is worth noting that the slight difference of energy gap between **1**–Zn and **1**–Cd may be responsible for different emission wavelength in the detection of Zn^{2+} and Cd^{2+}. Thus, after coordination with Zn^{2+} and Cd^{2+}, the LUMO of sensor **1** decreased strongly and led to stronger ICT effect, resulting in red shift in the emission wavelength.

4. Conclusions

In summary, a sensor for the selective detection of Zn^{2+} and Cd^{2+}in solution and solid using a simple amino–terpyridine compound **1** was developed. The detection limits were determined to be 0.184 μM for Zn^{2+} and 0.176 μM for Cd^{2+}. Sensor **1** can react with Zn^{2+} and Cd^{2+} to generate solid emission complexes that are responsible for the detection of Zn^{2+} and Cd^{2+} in solid. These results confirm that terpyridines can be used as a good receptor for the detection of Zn^{2+} and Cd^{2+}. However, new sensors based on terpyridines may be designed with better solubility in aqueous solution and high quantum yield for detection of ions and cell–imaging.

Supplementary Information

Detection limits of Zn^{2+} and Cd^{2+} (figures S1, S2), B-H plots of sensor **1** with Zn^{2+} and Cd^{2+} (figures S3, S4), Job's plots for Zn^{2+} and Cd^{2+} (figures S5, S6), UV-Vis titration of Cd^{2+} (figure S7), ^{1}H NMR spectra of complexes **4** and **5** (figures S8, S9) are given in the supporting information, available at www.ias.ac.in/chemsci.

Acknowledgements

Author thanks the Fundamental Research Funds for the Central Universities (No. 5001-852018) and General project of scientific research of the Education Department of Liaoning Province (No. L2015107).

References

1. Yang Y, Zhao Q, Feng W and Li F 2012 *Chem. Rev.* **113** 192
2. Li X, Gao X, Shi W and Ma H 2013 *Chem. Rev.* **114** 590
3. Liu Z, He W and Guo Z 2013 *Chem. Soc. Rev.* **42** 1568
4. Vallee B L and Auld D S 1990 *Biochemistry* **29** 5647
5. Berg J M and Shi Y 1996 *Science* **271** 1081

6. Voegelin A, Pfister S, Scheinost A C, Marcus M A and Kretzschmar R 2005 *Environ. Sci. Technol.* **39** 6616
7. Mendes A M S, Duda G P, Nascimento C W A d and Silva M O 2006 *Scientia Agricola* **63** 328
8. Satarug S, Baker J R, Urbenjapol S, Haswell-Elkins M, Reilly P E B, Williams D J and Moore M R 2003 *Toxicol. Lett.* **137** 65
9. Xu Z, Yoon J and Spring D R 2010 *Chem. Soc. Rev.* **39** 1996
10. Sun Z, Li H, Guo D, Sun J, Cui G, Liu Y, Tian Y and Yan S 2015 *J. Mater. Chem. C* **3** 4713
11. Xia S, Liu G and Pu S 2015 *J. Mater. Chem. C* **3** 4023
12. Lee J J, Lee S A, Kim H, Nguyen L, Noh I and Kim C 2015 *RSC Adv.* **5** 41905
13. Tan Y, Gao J, Yu J, Wang Z, Cui Y, Yang Y and Qian G 2013 *Dalton Trans.* **42** 11465
14. Jin F, Xu D-L, Zhu H-Z, Yan Y, Zheng J, Zhang J, Zhou H-P, Wu J-Y and Tian Y-P 2014 *Dyes Pigm.* **109** 42
15. Chao D and Fu W-F 2014 *Dalton Trans.* **43** 306
16. Lu X, Li X, Guo K, Wang J, Huang M, Wang J-L, Xie T-Z, Moorefield C N, Cheng S Z D, Wesdemiotis C and Newkome G R 2014 *Chem. –Eur. J.* **20** 13094
17. Chao D and Fu W-F 2013 *Chem. Commun.* **49** 3872
18. Liu Y, Guo J, Liu R, Wang Q, Jin X, Ma L, Lv W, Liu S, Yuan S and Zhu H 2015 *J. Lumin.* **157** 249
19. Tan Y, Liu M, Gao J, Yu J, Cui Y, Yang Y and Qian G 2014 *Dalton Trans.* **43** 8048
20. Hu Q, Tan Y, Liu M, Yu J, Cui Y and Yang Y 2014 *Dyes Pigm.* **107** 45
21. Goodall W and Williams J A G 2001 *Chem. Commun.* 2514
22. Li Y Q, Bricks J L, Resch-Genger U, Spieles M and Rettig W 2006 *J. Phys. Chem. A* **110** 10972
23. Resch-Genger U, Li Y Q, Bricks J L, Kharlanov V and Rettig W 2006 *J. Phys. Chem. A* **110** 10956
24. Wang J and Hanan G S 2005 *Synlett* **2005** 1251
25. Schlegel H B, Scuseria G E, Robb M A, Cheeseman J R, Scalmani G, Barone V, Mennucci B, Petersson G A, Nakatsuji H, Caricato M, Li X, Hratchian H P, Izmaylov A F, Bloino J, Zheng G, Sonnenberg J L, Hada M, Ehara M, Toyota K, Fukuda R, Hasegawa J, Ishida M, Nakajima T, Honda Y, Kitao O, Nakai H, Vreven T, Montgomery J A, Peralta J E, Ogliaro F, Bearpark M, Heyd J J, Brothers E, Kudin K N, Staroverov V N, Kobayashi R, Normand J, Raghavachari K, Rendell A, Burant J C, Iyengar S S, Tomasi J, Cossi M, Rega N, Millam J M, Klene M, Knox J E, Cross J B, Bakken V, Adamo C, Jaramillo J, Gomperts R, Stratmann R E, Yazyev O, Austin A J, Cammi R, Pomelli C, Ochterski Martin J W R L, Morokuma K, Zakrzewski V G, Voth G A, Salvador P, Dannenberg J J, Dapprich S, Daniels A D, Farkas Ö, Foresman J B, Ortiz J V, Cioslowski J and Fox D J, *Gaussian 09 Revision A.1* (Gaussian Inc.: Wallingford CT) (2009)
26. Gogoi A, Samanta S and Das G 2014 *Sens. Actuators, B* **202** 788